Machine learning Landau free energy potentials

Mauro Pulzone,[1,2] Natalya S. Fedorova,[1] Hugo Aramberri,[1] and Jorge Íñiguez-González[1,2]

[1]*Luxembourg Institute of Science and Technology (LIST), Avenue des Hauts-Fourneaux 5, L-4362 Esch/Alzette, Luxembourg*
[2]*Department of Physics and Materials Science, University of Luxembourg, Rue du Brill 41, L-4422 Belvaux, Luxembourg*

We show how to construct Landau-like free energy potentials using a machine-learning approach. For concreteness, we focus on perovskite oxide $PbTiO_3$, representative of a large class of materials that undergo non-reconstructive structural phase transitions; in this case, a proper ferroelectric transformation with improper ferroelastic features. We work with a training set obtained from Monte Carlo simulations based on an atomistic "second-principles" potential for $PbTiO_3$. We rely exclusively on data that would be experimentally accessible – i.e., temperature-dependent polarization and strain, both with and without external electric fields and stresses applied –, to explore scenarios where the training set could be obtained from laboratory measurements. We introduce a scheme that allows us to identify optimal polynomial models of the temperature-dependent free energy surface, mapped as a function of the homogeneous electric polarization and homogeneous strain. Typically, our method evaluates thousands of possible models, ranking them by accuracy and predictive power. Our results for $PbTiO_3$ show that a very simple polynomial – where only two parameters depend linearly on temperature – is sufficient to yield a correct description of the material's behavior. We thus validate the usual approximations made in phenomenological studies of phase transitions of this kind. Remarkably, the obtained models also capture the subtle couplings by which elastic strain controls key features of ferroelectricity in $PbTiO_3$ – i.e., the symmetry of the polar phase and the discontinuous character of the transition –, despite the fact that no effort was made to include such information in the training set. We emphasize the distinctive aspects of our methodology (which relies on an original form of validation step) by comparing it with the usual machine-learning approach for model construction. Our results illustrate how physically motivated models can have remarkable predictive power, even if they are derived from a limited amount of data. We argue that such "third-principles" models can be the basis for predictive macroscopic or mesoscopic simulations of ferroelectrics and other materials undergoing non-reconstructive structural transitions.

I. INTRODUCTION

Machine-learned interatomic potentials (MLIPs) or force fields (MLFFs) derived from Density Functional Theory (DFT) calculations are transforming the field of computational materials science. Various MLIP families already enable an accurate and efficient description of interatomic interactions, which in turn makes it possible to run nanoscale molecular dynamics simulations ($\sim$nm, $\sim$ns) in a customary manner. While many challenges remain ahead – e.g., to tackle problems that require an explicit treatment of electrons or magnetism –, progress in the past decade has been outstanding, and today several MLIP schemes compete to become the standard approach for performing most DFT studies.[1–8]

However, whenever we are dealing with mesoscale or macroscopic phenomena, we are typically interested in length and time scales of at least μm and μs, respectively, where simulations based on atomistic MLIPs are unfeasible because of their high computational cost. The theoretical approach to such problems typically relies on continuum field theories, and even on macroscopic models whenever the inhomogeneities in the system do not require an explicit consideration. Of particular interest are cases involving ferroic materials (ferromagnetic, ferroelectric, ferroelastic, and all related systems) that often present complex multidomain states that can nevertheless be treated – in a qualitative and quasi-quantitative satisfactory way – by relatively simple Ginzburg-Landau

(continuum) or Landau (macroscopic) theories.[9–12]

Ginzburg-Landau potentials for ferroics have traditionally been obtained by fitting to experimental data. In the case of ferroelectrics, which is our focus here, the homogeneous part of the potential (i.e., the Landau model) can be derived from the temperature dependence of the polarization and dielectric permittivity.[13,14] Then, constructing a Ginzburg-Landau model requires additional information about the energy cost of having spatial inhomogeneities in the electric polarization, which can be deduced, e.g., from the spatial extension of domain walls.[15,16] Critically, such potentials capture thermal effects – i.e., the temperature evolution of the relevant free energy landscape – in a way that is approximate but sufficient for many purposes.

There have been efforts to derive effective free energy potentials from first principles, as needed to run predictive mesoscopic simulations whenever experimental information is not available (e.g., for hypothetical materials). For example, several authors have proposed schemes to fit temperature-dependent Landau potentials using data from statistical calculations based on atomistic models derived from DFT.[17,18] Attempts have also been made to fit simple temperature-dependent Ginzburg-Landau potentials.[18] More complex Ginzburg-Landau potentials have also been derived from DFT, but in this case the existing applications are restricted to the limit of 0 K as far as we know.[19,20] While valuable, these efforts are somewhat limited. Indeed, we still lack a general and

automatic scheme to create free energy potentials that capture, with an accuracy that can be systematically improved, the temperature-dependent behavior of materials with arbitrarily complex interactions.

To do this, one could adopt a generic machine-learning (ML) approach. For example, if we wanted to learn the behavior of the macroscopic polarization and macroscopic strain in a ferroelectric, we could train a neural network that takes as input the environmental conditions (temperature, external pressure, external electric field) and produces as output the properties of interest (equilibrium polarization and strain). Such a scheme might not allow us to understand the underlying physical mechanisms responsible for the observed behavior, but it would enable accurate calculations of the properties of interest within the limits – of temperature and external fields – defined by the training set (TS).

However, in this context, it seems unwise to ignore the mentioned time-tested application of Landau-like free energy models, which has enabled a successful treatment of many intricate cases. With this in mind, here we explore a physics-informed ML approach that builds on such a key insight, i.e., that polynomial models of the free energy usually work very well to describe ferroelectricity and related or analogous phenomena. Our scheme automatically determines effective potentials capable of reproducing a TS of relevant thermodynamic information, deriving directly from the data which monomials (that is, coupling terms) need to appear in the Landau model. As we will show, not only does the proposed scheme reproduce accurately the data in the TS, but it also reveals covert couplings that yield non-trivial behaviors of the compound we investigate here as a relevant example, ferroelectric perovskite $PbTiO_3$.

The manuscript is organized as follow. In Section II we introduce the main ideas and formalism of the proposed machine-learning approach. In Section III we briefly justify the choice of $PbTiO_3$ as a relevant model material, introducing some of the non-trivial behaviors it presents. Here we also describe the second-principles calculations from which we obtain the training set. In Section IV we discuss the results of our fitting procedure; we first consider simple models that depend on the electric polarization alone, and then move to models that depend explicitly on both polarization and strain. In Section V we emphasize the non-trivial physical effects captured by our models, which highlight their predictive power. Here we also discuss how the present method relates to more traditional approaches in the ML model-building literature, emphasizing peculiarities that could be useful in other contexts. In Section V we also outline our envisioned path toward what we term "predictive third-principles simulations". We conclude in Section VI with a brief summary.

TABLE I. Symmetry-invariant couplings, involving polarization $\boldsymbol{P}$ and strain $\boldsymbol{\eta}$, that we consider in the Landau free energy potential of $PbTiO_3$. These invariants are the same for any perovskite compound provided one takes the ideal cubic phase ($Pm\bar{3}m$) as reference. Note that the A_β coefficients for the $f_\beta(\boldsymbol{P})$ terms could correspond to a full model $F(\boldsymbol{P}, \boldsymbol{\eta}; \boldsymbol{\mathcal{E}}, \boldsymbol{\sigma}, T)$ or to a renormalized model $\tilde{F}(\boldsymbol{P}; \boldsymbol{\mathcal{E}}, T)$; in the latter case, they would be written with a tilde, as $\tilde{A}_\beta$ (see text).

A_β	$f_\beta(\boldsymbol{P})$
A_{2i}	$P_x^2 + P_y^2 + P_z^2$
A_{4i}	$(P_x^2 + P_y^2 + P_z^2)^2$
A_{22}	$P_x^2 P_y^2 + P_x^2 P_z^2 + P_y^2 P_z^2$
A_{6i}	$(P_x^2 + P_y^2 + P_z^2)^3$
A_{42}	$P_x^4(P_y^2 + P_z^2) + P_y^4(P_x^2 + P_z^2) + P_z^4(P_y^2 + P_x^2)$
A_{222}	$P_x^2 P_y^2 P_z^2$
A_{8i}	$(P_x^2 + P_y^2 + P_z^2)^4$
A_{422}	$P_x^4 P_y^2 P_z^2 + P_x^2 P_y^4 P_z^2 + P_x^2 P_y^2 P_z^4$
A_{44}	$P_x^4 P_y^4 + P_x^4 P_z^4 + P_y^4 P_z^4$
A_{62}	$P_x^6 P_y^2 + P_x^6 P_z^2 + P_x^2 P_y^6 + P_x^2 P_z^6 + P_y^6 P_z^2 + P_y^2 P_z^6$

B_β	$f_\beta(\boldsymbol{P}, \boldsymbol{\eta})$
B_{12i}	$(\eta_{xx} + \eta_{yy} + \eta_{zz})(P_x^2 + P_y^2 + P_z^2)$
B_{12}	$\eta_{xx} P_x^2 + \eta_{yy} P_y^2 + \eta_{zz} P_z^2$
B_{14i}	$(\eta_{xx} + \eta_{yy} + \eta_{zz})(P_x^2 + P_y^2 + P_z^2)^2$
B_{14}	$\eta_{xx} P_x^4 + \eta_{yy} P_y^4 + \eta_{zz} P_z^4$
B_{122}	$(\eta_{xx} + \eta_{yy} + \eta_{zz})(P_x^2 P_y^2 + P_x^2 P_z^2 + P_y^2 P_z^2)$
B_{22i}	$(\eta_{xx} + \eta_{yy} + \eta_{zz})^2(P_x^2 + P_y^2 + P_z^2)$
B_{22}	$\eta_{xx}^2 P_x^2 + \eta_{yy}^2 P_y^2 + \eta_{zz}^2 P_z^2$
B_{112i}	$(\eta_{xx}\eta_{yy} + \eta_{xx}\eta_{zz} + \eta_{yy}\eta_{zz})(P_x^2 + P_y^2 + P_z^2)$
$B_{1'11}$	$\eta_{yz} P_y P_z + \eta_{xz} P_z P_x + \eta_{xy} P_x P_y$

C_β	$f_\beta(\boldsymbol{\eta})$
C_1	$\eta_{xx} + \eta_{yy} + \eta_{zz}$
C_2	$\eta_{xx}^2 + \eta_{yy}^2 + \eta_{zz}^2$
C_{11}	$\eta_{xx}\eta_{zz} + \eta_{yy}\eta_{xx} + \eta_{yy}\eta_{zz}$
$C_{2'}$	$\eta_{yz}^2 + \eta_{xz}^2 + \eta_{xy}^2$

II. OUR APPROACH

In this section we introduce the Landau treatment of ferroelectric phase transitions and related effects, taking the case of perovskite oxides as a representative and relevant example, a generalization being trivial. We then describe our proposed methodology to learn the Landau potential from a TS of standard thermodynamic data.

Let us note that here we are interested in describing the free energy landscape in a wide range of temperatures, and that the vicinity of the phase transition is not a particular concern for us. For this reason, and recognizing that Landau potentials were originally introduced to describe the transition region,[12,21] we often refer to our free energy models as being "Landau-like".

A. Landau-like model of a ferroelectric perovskite

We start by selecting the three-dimensional polarization vector, $\boldsymbol{P}$, as the main variable of interest, which we use to describe the state of the system. We want to study the associated free energy surface $\tilde{F} = \tilde{F}(\boldsymbol{P}; \boldsymbol{\mathcal{E}}, T)$, where T is the temperature and $\boldsymbol{\mathcal{E}}$ is the external electric field. The minima of $\tilde{F}$ represent equilibrium states of the material. In a Landau-like approach, $\tilde{F}$ is written as Taylor series for the order parameter around a suitable chosen reference phase with $\boldsymbol{P} = \boldsymbol{0}$. Formally, we have

$$\tilde{F}(\boldsymbol{P}; \boldsymbol{\mathcal{E}}, T) = \tilde{F}_0(T) + \sum_\beta \tilde{A}_\beta(T) f_\beta(\boldsymbol{P}) - \boldsymbol{\mathcal{E}} \cdot \boldsymbol{P} , \quad (1)$$

where $A_\beta(T)$ are temperature-dependent parameters and $f_\beta(\boldsymbol{P})$ are polynomial functions that are invariant under the symmetries of the reference phase. In the case of ferroelectric perovskites, the reference structure is the ideal cubic phase with $Pm\bar{3}m$ space group. The corresponding f_β polynomials are given in Table I up to the 8th order in the polarization. Note also the term $\tilde{F}_0(T)$, which describes free energy variations that do not depend on $\boldsymbol{P}$ or $\boldsymbol{\mathcal{E}}$; we will not discuss it here.

Strain is a key ingredient to describe ferroelectrics, as it participates in one of their most important properties: piezoelectricity. Further, many ferroelectrics – certainly perovskites like $PbTiO_3$ – are highly sensitive to mechanical stress.[22] To account for such effects, we need a Landau potential that includes strains as variables and stresses as fields. We formally have

$$F(\boldsymbol{P}, \boldsymbol{\eta}; \boldsymbol{\mathcal{E}}, \boldsymbol{\sigma}, T) = F_0(T) + \sum_\beta A_\beta(T) f_\beta(\boldsymbol{P}) + \sum_\beta B_\beta(T) f_\beta(\boldsymbol{P}, \boldsymbol{\eta}) + \sum_\beta C_\beta(T) f_\beta(\boldsymbol{\eta}) - \boldsymbol{\mathcal{E}} \cdot \boldsymbol{P} - \boldsymbol{\sigma} \cdot \boldsymbol{\eta} , \qquad (2)$$

where $\boldsymbol{\eta}$ and $\boldsymbol{\sigma}$ are the symmetric strain and stress tensors, respectively; we denote the corresponding tensor components as $\boldsymbol{\eta} = (\eta_{xx}, \eta_{yy}, \eta_{zz}, \eta_{yz}, \eta_{xz}, \eta_{xy})$. Here, $f_\beta(\boldsymbol{P}, \boldsymbol{\eta})$ and $f_\beta(\boldsymbol{\eta})$ are symmetry-invariant polynomials analogous to $f_\beta(\boldsymbol{P})$, while $B_\beta(T)$ and $C_\beta(T)$ are their corresponding coefficients. Table I lists the polarization, strain, and strain-polarization invariants considered in this work.

It is important to note that the Landau potentials introduced above are related in the following way:

$$\tilde{F}(\boldsymbol{P}; \boldsymbol{\mathcal{E}}, T) = \min_{\boldsymbol{\eta}} F(\boldsymbol{P}, \boldsymbol{\eta}; \boldsymbol{\mathcal{E}}, \boldsymbol{\sigma} = \boldsymbol{0}, T) . \qquad (3)$$

This implies that, when we work with $\tilde{F}$, the strain is treated as a slave variable that follows the polarization. A related subtlety about Eqs. (1) and (2) is that some seemingly equivalent coefficients have a tilde in the former but not in the latter, as they are in fact different quantities. Thus, for example, we would say that the parameter $\tilde{A}_\beta$ is the *strain-renormalized* version of A_β.

As indicated in the equations above, all the parameters in our models (e.g., $A_\beta(T)$, $B_\beta(T)$, etc.) are in principle T-dependent. For a generic coefficient $\phi_\beta(T)$, we express such a dependence as the following Taylor series

$$\phi_\beta(T) = \phi_\beta^{(0)} + \phi_\beta^{(1)} T + \phi_\beta^{(2)} T^2 + \cdots , \qquad (4)$$

which defines the new T-independent coefficients $\phi_\beta^{(n)}$.

Table I lists all the f_β interaction terms, and associated ϕ_β parameters, considered in this work. (Some extensions, to address specific points, are discussed below.) We truncate the order of the expansion in a way that depends on the nature of the couplings, allowing for a more detailed description of the energetics of the

primary order parameter, that is, the polarization $\boldsymbol{P}$ in our sample problem. Specifically, for the terms involving the polarization alone, $f_\beta(\boldsymbol{P})$, we consider all symmetry-independent couplings up to the 8th order. For the strain terms, $f_{\beta(\boldsymbol{\eta})}$, we stop at the quadratic order. Finally, as regards the polarization-strain couplings $f_\beta(\boldsymbol{P}, \boldsymbol{\eta})$, we go up to a relatively high order ($\sim \eta P^4$, $\sim \eta^2 P^2$) when the linear strains are involved, but consider only the lowest-order couplings ($\sim \eta P^2$) for shear strains. Similarly, when it comes to the T-dependence of the coefficients, we consider a more detailed treatment of those associated to the $f_\beta(\boldsymbol{P})$ and $f_\beta(\boldsymbol{\eta})$ couplings, while we are more restrictive when treating the $f_\beta(\boldsymbol{P}, \boldsymbol{\eta})$ terms. The number of models considered is thus limited by these truncations and some additional simplifications – e.g., we always include the $\tilde{A}_{2i}^{(0)}$ and $\tilde{A}_{2i}^{(1)}$ coefficients in all our models, we always include the $C_1^{(0)}$, $C_1^{(1)}$, $C_2^{(0)}$, $C_{2'}^{(0)}$ and $B_{2',11}^{(0)}$ couplings in all our $F(\boldsymbol{P}, \boldsymbol{\eta})$ models, etc. Furthermore, we truncate the temperature expansion at the linear term. For the higher-order couplings ($\sim \eta P^4$, $\sim \eta^2 P^2$), we assume no temperature dependence. Despite these restrictions, we work with a very large universe of possible potentials: we evaluate over 16 000 inequivalent models of the $\tilde{F}(\boldsymbol{P})$ type, while we consider over 69 000 different $F(\boldsymbol{P}, \boldsymbol{\eta})$ models with up to 17 parameters.

B. Machine learning the Landau potential

We now discuss our approach to compute Landau free energy potentials. First, we present how a given model – as defined by a specific combination of $\phi_\beta^{(n)}$ parameters – is fitted to a TS of data. Then, we introduce the way in which we identify optimal models – simple, yet accu-

rate and predictive – from the vast universe of possible potentials.

1. Fitting the parameters of a particular model

Suppose we are given a training set $\mathcal{D}$ of the form

$$\mathcal{D} = \left\{ \{T^{(s)}, \boldsymbol{\mathcal{E}}^{(s)}, \boldsymbol{\sigma}^{(s)}; \mathbf{P}^{(s)}, \boldsymbol{\eta}^{(s)}\} \right\} , \qquad (5)$$

where $s = 1, ..., n$ runs over representative equilibrium configurations. Hence, this TS describes how the state of the system – as characterized by its polarization and strain – depends on the external conditions of temperature, electric field and stress. For convenience, in the following we assume that all the quantities in the TS are scaled in a physically meaningful way, which we describe in Section III C, so they are dimensionless.

The model $F(\boldsymbol{P}, \boldsymbol{\eta}; \boldsymbol{\mathcal{E}}, \boldsymbol{\sigma}, T)$ must be such that the configurations in $\mathcal{D}$ are predicted to be equilibrium states. Mathematically, this implies the model must satisfy the equations of state

$$\nabla_{\boldsymbol{P}} F \Big|_{\mathrm{eq}} = \mathbf{0} \qquad (6)$$

and

$$\nabla_{\boldsymbol{\eta}} F \Big|_{\mathrm{eq}} = \mathbf{0} , \qquad (7)$$

where we use the notation

$$\nabla_{\boldsymbol{P}} = (\partial_{P_x}, \partial_{P_y}, \partial_{P_z}) \qquad (8)$$

and

$$\nabla_{\boldsymbol{\eta}} = (\partial_{\eta_{xx}}, \partial_{\eta_{yy}}, \partial_{\eta_{zz}}, \partial_{\eta_{yz}}, \partial_{\eta_{xz}}, \partial_{\eta_{xy}}) . \qquad (9)$$

We thus have a total of 9 equations, 3 for the polarization components and 6 for the strain components. By using F as given in Eq. (2), we get

$$\sum_{\beta}^{p(A)} A_{\beta}(T^{(s)}) \nabla_{\boldsymbol{P}} f_{\beta}(\mathbf{P}) \Big|_{\boldsymbol{P}^{(s)}} + \\ + \sum_{\beta}^{p(B)} B_{\beta}(T^{(s)}) \nabla_{\boldsymbol{P}} f_{\beta}(\mathbf{P}, \boldsymbol{\eta}) \Big|_{\boldsymbol{P}^{(s)}, \boldsymbol{\eta}^{(s)}} = \boldsymbol{\mathcal{E}}^{(s)} \qquad (10)$$

and

$$\sum_{\beta}^{p(C)} C_{\beta}(T^{(s)}) \nabla_{\boldsymbol{\eta}} f_{\beta}(\boldsymbol{\eta}) \Big|_{\boldsymbol{\eta}^{(s)}} + \\ + \sum_{\beta}^{p(B)} B_{\beta}(T^{(s)}) \nabla_{\boldsymbol{\eta}} f_{\beta}(\mathbf{P}, \boldsymbol{\eta}) \Big|_{\boldsymbol{P}^{(s)}, \boldsymbol{\eta}^{(s)}} = \boldsymbol{\sigma}^{(s)} , \qquad (11)$$

where we explicitly indicate that we can construct such relations for all $s = 1, ..., n$ states in $\mathcal{D}$. Here we also introduce $p(A)$, $p(B)$ and $p(C)$ as the number of A_{β}, B_{β} and C_{β} parameters, respectively, in the model being considered. Hence, we have $N = 9n$ linear equations and $p = p(A) + p(B) + p(C)$ unknowns, which will typically yield an overdetermined system.

For convenience, we express the system of equations using the matrix notation

$$\underline{\underline{\mathbf{M}}}\boldsymbol{\phi} = \boldsymbol{y} , \qquad (12)$$

where $\boldsymbol{y}$ is a vector of dimension N that contains the right-hand side of the equations of state, that is, 3 electric field components and 6 stress components for each of the n states in $\mathcal{D}$. Then, $\boldsymbol{\phi}$ is a vector of dimension p that contains the ϕ_{β} coefficients to be fitted. Finally, $\underline{\underline{\mathbf{M}}}$ is a matrix of dimensions $N \times p$ that is populated with the derivatives – with respect to polarization and strain components – of the f_{β} invariants.

Such an overdetermined system of equations does not have an exact solution. Hence, we fit the coefficients $\boldsymbol{\phi}$ so as to minimize the discrepancy between the left- and right-hand sides of Eq. (12). To this end, we introduce the error function

$$\mathsf{E}(\boldsymbol{\phi}) = \frac{1}{N} ||\underline{\underline{\mathbf{M}}}\boldsymbol{\phi} - \boldsymbol{y}||^2 . \qquad (13)$$

If we minimize this quantity with respect to $\boldsymbol{\phi}$, by solving for $\partial_{\boldsymbol{\phi}}\mathsf{E} = 0$, we obtain a solution known as the normal equation:[23]

$$\boldsymbol{\phi}_{\mathrm{min}} = (\underline{\underline{\mathbf{M}}}^T \underline{\underline{\mathbf{M}}})^{-1} \underline{\underline{\mathbf{M}}}^T \boldsymbol{y} . \qquad (14)$$

Hence, we take advantage of the fact that Landau potentials are linear in the parameters to be fitted, which makes it possible to estimate their values by solving a simple polynomial regression. Thus, the calculation of the parameters of a given Landau model is exact and very fast.

2. Selecting the best Landau model

We are left with the task of selecting an optimum Landau potential from the thousands of variants we can easily generate and fit. Our optimum potential should be as simple as possible (to facilitate our physical understanding of the dominant effects) while being sufficiently accurate (i.e., we want a small $\mathsf{E}(\boldsymbol{\phi_{\mathrm{min}}})$) and predictive (i.e., we want our potential to be as reliable as possible when applied to situations not considered in the TS).

As it is known, minimizing an error function like our $\mathsf{E}(\boldsymbol{\phi})$ is not a sufficient criterion to decide how many (and which) couplings to include in a model potential, as this will typically lead to overfitting and a reduced predictive power of the resulting overly-complex models. Then, our experience with cross-validation schemes – both from this work and previous related studies[24] – is not convincing, as we find that the usual approaches (from the simple
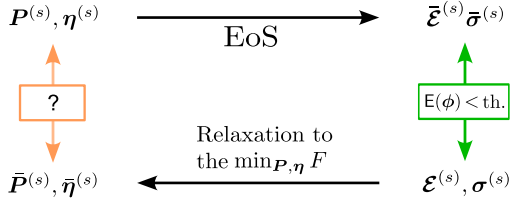
FIG. 1. Sketch illustrating our fitting and validation procedures, and how the latter tests the predictive power of the models (see text).

"leave-p-out" method[25] to consideration of a proper validation set of data equivalent to those in the TS) yield models that seem unnecessarily complex and offer poor predictive power.

Here we introduce our own validation scheme, designed to test the models' predictive power in a way that, while restricted, proves effective. Figure 1 helps illustrate our approach. Given a model defined by $\phi_{\min}$, we can use the information about an equilibrium state, $\{\boldsymbol{P}^{(s)}, \boldsymbol{\eta}^{(s)}; T^{(s)}\}$, to derive the corresponding external fields from Eqs. (10) and (11). We express such fields as

$$\bar{\boldsymbol{\mathcal{E}}}^{(s)} = \boldsymbol{\mathcal{E}}[\mathbf{P}^{(s)}, \boldsymbol{\eta}^{(s)}; T^{(s)}] \tag{15}$$

and

$$\bar{\boldsymbol{\sigma}}^{(s)} = \boldsymbol{\sigma}[\mathbf{P}^{(s)}, \boldsymbol{\eta}^{(s)}; T^{(s)}] \, . \tag{16}$$

As indicated in Fig. 1, the model parameters are computed to minimize the differences between $\{\boldsymbol{\mathcal{E}}^{(s)}, \boldsymbol{\sigma}^{(s)}\}$ and $\{\bar{\boldsymbol{\mathcal{E}}}^{(s)}, \bar{\boldsymbol{\sigma}}^{(s)}\}$. Hence, if our model is accurate, we can expect these quantities to be close.

Interestingly, because we are dealing with equilibrium states, we can also go in the opposite direction: given $\{\boldsymbol{\mathcal{E}}^{(s)}, \boldsymbol{\sigma}^{(s)}, T^{(s)}\}$, we can run a numerical simulation to find the minimum of the potential $F(\boldsymbol{P}, \boldsymbol{\eta}; \boldsymbol{\mathcal{E}}^{(s)}, \boldsymbol{\sigma}^{(s)}, T^{(s)})$. Let us write the solution as

$$\bar{\boldsymbol{P}}^{(s)} = \boldsymbol{P}[\boldsymbol{\mathcal{E}}^{(s)}, \boldsymbol{\sigma}^{(s)}, T^{(s)}] \tag{17}$$

and

$$\bar{\boldsymbol{\eta}}^{(s)} = \boldsymbol{P}[\boldsymbol{\mathcal{E}}^{(s)}, \boldsymbol{\sigma}^{(s)}, T^{(s)}] \, . \tag{18}$$

Noting that the Landau potential will typically present multiple minima, it is convenient to start the mentioned minimization from $\{\boldsymbol{P}^{(s)}, \boldsymbol{\eta}^{(s)}\}$, i.e., the actual state in the TS. Next, we introduce the new error function

$$\mathsf{e} = \max_{s} \|\boldsymbol{P}^{(s)} - \bar{\boldsymbol{P}}^{(s)}\| + \max_{s} \|\boldsymbol{\eta}^{(s)} - \bar{\boldsymbol{\eta}}^{(s)}\| \, , \tag{19}$$

recalling that we are using rescaled dimensionless quantities (more in Section III C). This error function quantifies the difference between $\{\boldsymbol{P}^{(s)}, \boldsymbol{\eta}^{(s)}\}$ and $\{\bar{\boldsymbol{P}}^{(s)}, \bar{\boldsymbol{\eta}}^{(s)}\}$; thus, it allows us to test the predictive error of a model.

While this may seem a trivial exercise, we find it proves very effective to detect (and discard) deficient models.

For example, whenever an excessively complex potential presents spurious local minima, large values of e are usually obtained. Also, whenever the potential is very flat – e.g., close to the ferroelectric phase transition –, the error function E has difficulty to capture the local minima, as local maxima also satisfy the equilibrium condition; in such cases, seemingly sound models may render small values of $\mathsf{E}(\phi_{\min})$ but comparatively large values of e.

Indeed, as shown below, we find that minimizing this new error function constitutes the best strategy to identify optimum models in a reliable and automatic manner. Admittedly, the procedure is computationally heavier than a simple validation step, as it involves a large number of free energy minimizations. Yet, given the relative simplicity of our Landau potentials – compared to, e.g., atomistic force fields –, it remains affordable using standard desktop computers. Let us also stress that this validation procedure takes advantage of a specific feature of the TS we use here, namely, that all the states in $\mathcal{D}$ are equilibrium configurations that have a (local) minimum of the free energy associated to them. By contrast, in the usual MLIP approaches, the TS is composed of non-equilibrium configurations that are not minima of any energy function; hence, in principle, an analogous test of the predictive power of a machine-learned interatomic potential would not be possible.

III. NUMERICAL APPLICATION

In this section we justify our choice of $PbTiO_3$ as a convenient material to illustrate our method. Then, we describe how we generate the dataset $\mathcal{D}$ and the second-principles atomistic model used for that purpose. Finally, we specify the way in which we rescale the quantities entering the Landau potential.

A. Ferroelectric $PbTiO_3$

We work with ferroelectric perovskite oxide $PbTiO_3$ (PTO) to illustrate our methodology. PTO is a very relevant material, both scientifically and technologically, and remains one of the best studied ferroelectrics.[26] Further, it provides us with a test case that is both challenging (as regards the subtle physical couplings involved) and formally simple (because of the high symmetry, $Pm\bar{3}m$, of the reference $\boldsymbol{P} = \boldsymbol{0}$ phase).

Experimentally, PTO displays a discontinuous ferroelectric transition, at $T_C = 760$ K, between a cubic paraelectric phase (with space group $Pm\bar{3}m$) and a tetragonal ferroelectric phase ($P4mm$).[14] The spontaneous polarization is accompanied by a significant lattice deformation, as the unit cell develops a c/a aspect ratio of about 1.07 at room temperature. Accordingly, DFT studies evidence a strong coupling of polarization and strain.[27] For example, and most remarkably, it has been predicted[28] that, if a temperature-independent cubic cell (i.e., $\boldsymbol{\eta} = \boldsymbol{0}$) is im-

posed, PTO undergoes a continuous ferroelectric phase transition, at a much reduced temperature, to a phase that is rhombohedral ($R3m$) instead of tetragonal. (In these conditions, PTO is predicted to undergo an additional transition, at a lower temperature, to another rhombohedral ($R3c$) structure that resembles the most common phase of $BiFeO_3$.[28] Treating this case within a Landau approach would require considering extra order parameters in our model – i.e., octahedral tilts – and we do not consider it here.) Let us stress that these are highly non-trivial behaviors that stem from the complex multi-minima energy landscape of PTO. Hence, this material poses a singular challenge to our method for computing free energy potentials. Indeed, such peculiar conditions (e.g., $\boldsymbol{\eta} = \mathbf{0}$) will not be part of our TS and, thus, it is an open and intriguing question whether our potentials will capture the mentioned effects.

B. Atomistic simulations and training set

To generate the training set $\mathcal{D}$, we employ the "second-principles" atomistic effective potential for PTO described in Ref. 28. This model has been used in numerous studies of PTO and related compounds (e.g., PTO-based superlattices), and it has been shown to reproduce the behavior of the material in a way that is qualitatively and quasi-quantitatively correct.[29–33] The only noteworthy discrepancy between the model predictions and experimental results concerns the quantification of the ferroelectric transition temperature: for bulk PTO, Monte Carlo simulations using the second-principles model yield $T_C \approx 510$ K, while the experimental Curie point occurs at 760 K.[28] While significant, this disagreement is irrelevant in the current context, as we are not concerned by agreement with experiment. Here our focus is on capturing non-trivial thermodynamic behaviors using simple Landau-like potentials, and our atomistic model for PTO does capture many such complex behaviors.

It is worth noting here that our second-principles model for PTO involves a relatively low-order expansion of the energy around a cubic reference structure: up to the 4th order for the terms that depend on atomic displacements alone, quadratic in the terms related to strains alone, and with strain-phonon couplings that are linear in strain and quadratic in the atomic displacements.[28] Such a low-order model is nevertheless capable of reproducing non-trivial effects, such as PTO's weakly first-order phase transition, whose description is known to require a 6th-order free energy potential $\tilde{F}$.[13,21] This is an example of how the free energy landscape for the polarization gets renormalized by thermal fluctuations and by averaging over all non-essential atomic degrees of freedom, yielding behaviors that may not be immediately obvious from the form of the underlying atomic interactions. This point is discussed in some detail in Refs. 17 and 34.

To compute the equilibrium properties of bulk PTO at varying values of temperature, electric field and stress, we solve our second-principles model using Monte Carlo (MC) simulations. We typically work with a supercell that is a $10 \times 10 \times 10$ repetitions of the elemental perovskite 5-atom unit, thus corresponding to 5 000 atoms, assuming periodic boundary conditions. Close to the computed transition temperature, between 460 K and 550 K, we increase the supercell size to $12 \times 12 \times 12$, corresponding to 8 640 atoms, to mitigate finite-size effects. For each case considered, we perform 10 000 MC sweeps for thermalization of the system, followed by 40 000 sweeps to calculate the thermal averages of polarization and strain. We checked that these choices yield sufficiently converged results. Typically, at each temperature considered, we first solve the case where the external fields are set to zero, and use a configuration characteristic of the corresponding equilibrium state as the starting point of the calculations with fields applied.

We build two training sets, $\tilde{\mathcal{D}}$ and $\mathcal{D}$, to train the $\tilde{F}(\boldsymbol{P}; \boldsymbol{\mathcal{E}}, T)$ and $F(\boldsymbol{P}, \boldsymbol{\eta}; \boldsymbol{\mathcal{E}}, \boldsymbol{\sigma}, T)$ models, respectively. To build $\tilde{\mathcal{D}}$ we consider 21 different temperatures ranging from 50 K to 1000 K, with a higher concentration of temperatures close to T_C. For each temperature, we consider 27 cases with an electric field applied (and zero applied stress); the field components are chosen randomly with a maximum magnitude of 100 MV/m. All the states in $\tilde{\mathcal{D}}$ are obtained in zero-stress conditions. For the second training set, $\mathcal{D}$, we consider 7 temperatures ranging from 100 K to 700 K. For each temperature we include the corresponding zero-stress states contained in $\tilde{\mathcal{D}}$. Additionally, for each temperature we include 12 cases with applied external stress (and zero applied electric field); the stress components are randomly chosen with a maximum magnitude of 1 GPa. All in all, $\tilde{\mathcal{D}}$ contains 567 entries corresponding to equilibrium states at zero stress, yielding 1 701 equilibrium relations (Eq. (10)). Meanwhile, $\mathcal{D}$ consists of 273 entries, yielding 2 457 relations (Eqs. (10) and (11)).

C. Dimensionless quantities

It is convenient to use natural scales for the various physical variables involved in the problem, so as to work with dimensionless magnitudes. This allows us to combine the errors associated to different quantities, as e.g. done in Eqs. (13) and (19) for electric and elastic variables.

We thus rescale energy and polarization so that the tetragonal ground state of our simulated bulk PTO (in the limit of 0 K) has an energy $\Delta F = F - F_0 = -1$ and a polarization $P_z = 1$. We further rescale the temperatures so that $T_C = 1$. As for the strains, they are dimensionless by definition and we find it appropriate to not rescale them at all. The actual values of energy, polarization, and temperatures can be recovered by simply noting that the unscaled quantities are: $\Delta F = -4.64$ GJ m^{-3}, $P_z = 0.992$ C m^{-2} and $T_C = 510$ K.

As discussed below, we checked these choices and found it unnecessary to further weight the electric and elastic contributions to our error functions. Thus, the scalings just described enable a balanced fit that treats well all the variables in the problem. Note that this conclusion might be specific of the problem studied in this work; the scaling of the variables in the model should be considered on a case-by-case basis. As a default strategy, one could use the corresponding standard deviation in the TS data as a natural scale for each variable involved in the free energy model. Such a choice seems to render robust results in MLIP training schemes that combine errors in energy, forces and stresses.[3]

IV. RESULTS

We discuss first Landau potentials that are functions of the polarization alone, then potentials where strains are explicitly treated.

A. $\tilde{F}(\mathbf{P}; \boldsymbol{\mathcal{E}}, T)$ models

Since these models do not treat strain explicitly, they cannot reproduce the dependence of the system's properties as a function of stress. Hence, to fit $\tilde{F}(\mathbf{P}; \boldsymbol{\mathcal{E}}, T)$ models, we use the zero-stress data in $\tilde{\mathcal{D}}$ defined above. Similarly, the error functions $\tilde{\mathsf{E}}$ and $\tilde{\mathsf{e}}$ are obtained from Eqs. (13) and (19), respectively, by leaving out the contributions from stress and strain.

As described in Section II, our procedure consists in fitting all possible models up to the 8th order; that is, we consider all possible combinations of the invariants $f_\beta(\boldsymbol{P})$ in Table I, albeit the mentioned simplifications (e.g., the $\tilde{A}_{2i}^{(0)}$ and $\tilde{A}_{2i}^{(1)}$ parameters are always included). Our results are summarized in Fig. 2(a), from which we can draw two main conclusions. On the one hand, the average error $\tilde{\mathsf{E}}$ tends to decrease as we increase the number of parameters in the model, but with a large spread for models with the same number of couplings. On the other hand, we obtain remarkably accurate models with a relatively small number of parameters.

For the sake of the argument, let us consider a model to be reasonably accurate if $\tilde{\mathsf{E}} < 10^{-4}$. This threshold, marked with a dashed line in Fig. 2(a), corresponds to having electric fields reproduced to within 5 MV m^{-1} – i.e., 1/20 times the largest applied field considered in our TS –, which would seem sufficient for most use cases. (Having thermodynamic properties predicted to within a 5 % is, at least, on par with the accuracy of present first-principles methods.) Then, models with as few as 4 parameters already give an acceptable description of our data. For example, this is the case of the model labeled
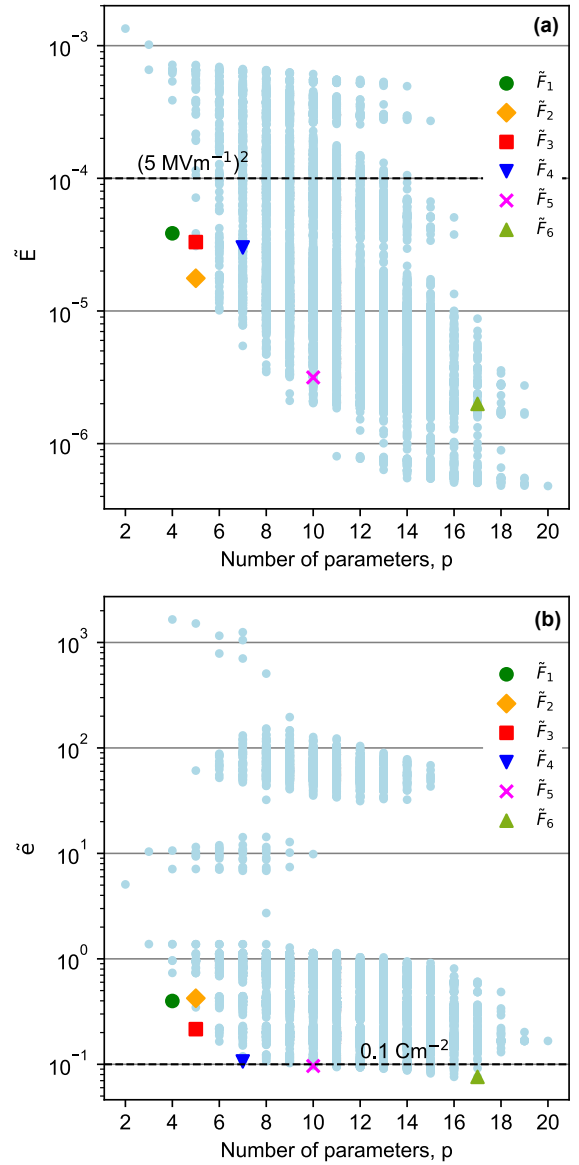

FIG. 2. (a) Error function $\tilde{\mathsf{E}}$ as a function of the number of parameters in the model (p). (b) Predictive error $\tilde{\mathsf{e}}$ as a function of p. Coloured symbols highlight the selected models, from F_1 to F_6, discussed in the text. Error thresholds mentioned in the text are indicated with dashed lines.

$\tilde{F}_1$ in Fig. 2(a), which is given by

$$\begin{aligned}
\tilde{F}_1 &= (\tilde{A}_{2i}^{(0)} + \tilde{A}_{2i}^{(1)} T)(P_x^2 + P_y^2 + P_z^2) \\
&+ \tilde{A}_{22}^{(0)}(P_x^2 P_y^2 + P_x^2 P_z^2 + P_y^2 P_z^2) \\
&+ \tilde{A}_{6i}^{(0)}(P_x^2 + P_y^2 + P_z^2)^3 \,,
\end{aligned} \tag{20}$$

and for which we report the fitted parameters in Table II. The accuracy of this simple model in reproducing $\tilde{\mathcal{D}}$ can be better appreciated in Suppl. Fig. 1. This figure also shows the result for the best 5-parameter model identified by our method, labeled $\tilde{F}_2$ in Fig. 2(a), which includes the same couplings as $\tilde{F}_1$ plus the $\tilde{A}_{42}^{(0)}$ term (see Table II).
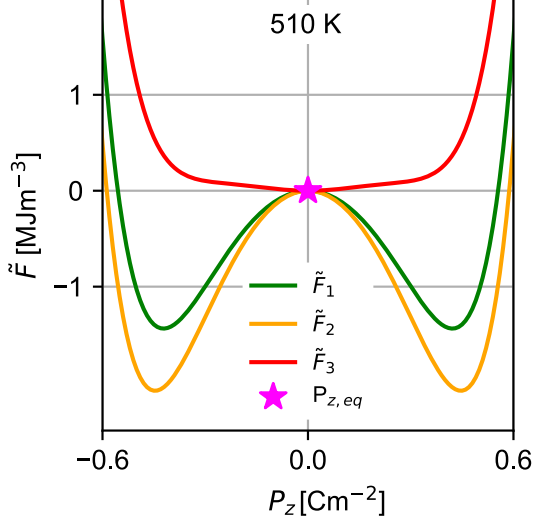
FIG. 3. Free energy landscape as a function of P_z (for $P_x = P_y = 0$) at $T = 510$ K and $\boldsymbol{\mathcal{E}} = \mathbf{0}$ for models $\tilde{F}_1$, $\tilde{F}_2$, and $\tilde{F}_3$ (see text). The magenta star indicates the equilibrium polarization $P_{z,eq}$ present in the TS. Note that the free energy and polarization are given in SI units.

FIG. 4. Equilibrium polarization as a function of temperature with $\boldsymbol{\mathcal{E}} = \mathbf{0}$. The grey data points represent values obtained from second-principles Monte Carlo simulations and are part of our dataset, while the red and blue curves correspond to the predictions of models $\tilde{F}_3$ and $\tilde{F}_4$, respectively. Note that the polarization and temperature are given in SI units.

Hence, if we take the error function $\tilde{\mathsf{E}}$ as our sole quality criterion, models $\tilde{F}_1$ and $\tilde{F}_2$ would seem sufficient choices to describe PTO.

However, as mentioned in Section II, minimizing $\tilde{\mathsf{E}}$ does not guarantee the predictive power of our models, as illustrated by the following example. Let us consider three models, the already mentioned $\tilde{F}_1$ and $\tilde{F}_2$ as well as an additional 5-parameter model labeled $\tilde{F}_3$ in Fig. 2(a). Figure 3 shows the free energy as a function of P_z (and for $P_x = P_y = 0$) given by these three models at $T = 510$ K, right above the ferroelectric transitions temperature predicted by our atomistic simulations. We know that, at this temperature and for zero applied electric field, the equilibrium polarization of the material is zero, i.e., the Landau potential should have a minimum at the origin. However, models $\tilde{F}_1$ and $\tilde{F}_2$ render a double well potential, with a maximum at $\mathbf{P} = \mathbf{0}$, a qualitatively incorrect result. By contrast, model $\tilde{F}_3$ – which has a bigger error $\tilde{\mathsf{E}}$ than model $\tilde{F}_2$ – predicts a very flat energy landscape with a minimum at the origin. Indeed, as regards predicting the behavior of the material near T_C in a qualitatively correct way, $\tilde{F}_3$ clearly outperforms $\tilde{F}_2$. Next we show how we can identify and select such reliable models automatically.

To do this, we use the second error function, $\tilde{\mathsf{e}}$ (Eq. (19)), introduced in Section II B 2, which quantifies the models' ability to predict the equilibrium states of the TS by energy minimization. Our results are summarized in Fig. 2(b). According to this new criterion, $\tilde{F}_3$ is the best choice of 5-parameter model, while the performance of $\tilde{F}_2$ is relatively modest. If we set $\tilde{\mathsf{e}} < 10^{-1}$ as the threshold for accuracy – which corresponds to a
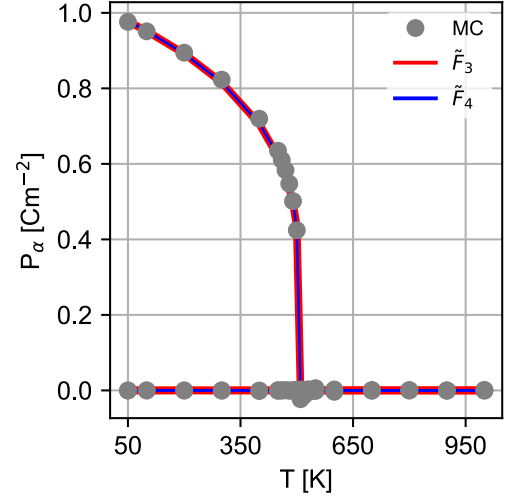
maximum error of about 0.1 C m^{-2} for the predicted polarization –, we find that the model labeled $\tilde{F}_4$ (10 parameters, see Table II) is the simplest model that complies with our requirements.

It is worth noting that the predictive error $\tilde{\mathsf{e}}$ allows us to identify the level of complexity beyond which our models do not improve. Indeed, Fig. 2(b) includes results for 156 different models of 17 parameters, as well as 55 different models of more than 17 parameters. We find that, beyond 17 independent couplings, $\tilde{\mathsf{e}}$ starts to grow with the number of parameters, the absolute best model being the one labeled $\tilde{F}_6$. Indeed, models with more than 17 parameters continue to improve their accuracy, as shown in Fig. 2(a), but yield increasingly worse predictions, as shown in Fig. 2(b).

The prediction error $\tilde{\mathsf{e}}$ quantifies the maximum discrepancy across the entire dataset. As mentioned above, cases where the free energy surface is very flat – most notably, close to T_C – can be expected to be particularly challenging. This can be appreciated in Supp. Fig. 2, where we show the maximum prediction error as a function of temperature. By examining these detailed results, we can finetune the choice of Landau model according to our needs in particular applications. For example, if we are interested in describing PTO in a broad temperature range, and if it is sufficient to have a qualitatively correct description of the transition region, $\tilde{F}_3$ might be our

TABLE II. Parameters for selected $\tilde{F}(\boldsymbol{P}; \boldsymbol{\mathcal{E}}, T)$ models given in SI units.

	Parameter	Units	$\tilde{F}_1$	$\tilde{F}_2$	$\tilde{F}_3$	$\tilde{F}_4$	$\tilde{F}_5$	$\tilde{F}_6$
T-independent terms	$\tilde{A}_{2i}^{(0)}$	10^8 C^{-2} m^2 N	-3.94679	-4.02122	-3.75628	-3.63736	-3.20683	-3.35136
	$\tilde{A}_{4i}^{(0)}$	10^8 C^{-4} m^6 N			-0.27596	-0.56378	-1.97729	-1.17002
	$\tilde{A}_{22}^{(0)}$	10^8 C^{-4} m^6 N	2.92026	4.22073	2.92379	2.73622	3.19689	1.59453
	$\tilde{A}_{6i}^{(0)}$	10^8 C^{-6} m^{10} N	1.34097	1.38310	1.47317	1.62257	2.46231	1.40375
	$\tilde{A}_{42}^{(0)}$	10^8 C^{-6} m^{10} N		-1.98136			1.50262	4.01424
	$\tilde{A}_{222}^{(0)}$	10^8 C^{-6} m^{10} N				7.76192		15.87736
	$\tilde{A}_{8i}^{(0)}$	10^8 C^{-8} m^{14} N						0.42261
	$\tilde{A}_{422}^{(0)}$	10^8 C^{-8} m^{14} N						-16.10410
	$\tilde{A}_{44}^{(0)}$	10^8 C^{-8} m^{14} N					-5.02926	-4.20465
	$\tilde{A}_{62}^{(0)}$	10^8 C^{-8} m^{14} N					-2.66843	-3.80982
T-dependent terms	$\tilde{A}_{2i}^{(1)}$	10^6 C^{-2} m^2 N K^{-1}	0.74973	0.75719	0.74130	0.72655	0.65142	0.66895
	$\tilde{A}_{4i}^{(1)}$	10^6 C^{-4} m^6 N K^{-1}				0.02726	0.25120	0.15726
	$\tilde{A}_{22}^{(1)}$	10^6 C^{-4} m^6 N K^{-1}						0.15596
	$\tilde{A}_{6i}^{(1)}$	10^6 C^{-6} m^{10} N K^{-1}					-0.09493	-0.02123
	$\tilde{A}_{222}^{(1)}$	10^6 C^{-6} m^{10} N K^{-1}						0.23905
	$\tilde{A}_{422}^{(1)}$	10^6 C^{-8} m^{14} N K^{-1}						-2.36708
	$\tilde{A}_{44}^{(1)}$	10^6 C^{-8} m^{14} N K^{-1}						-1.21606

optimal choice. This model is given by

$$
\begin{aligned}
\tilde{F}_3 = {} & (\tilde{A}_{2i}^{(0)} + \tilde{A}_{2i}^{(1)} T)(P_x^2 + P_y^2 + P_z^2) \\
& + \tilde{A}_{4i}^{(0)}(P_x^2 + P_y^2 + P_z^2)^2 \\
& + \tilde{A}_{22}^{(0)}(P_x^2 P_y^2 + P_x^2 P_z^2 + P_y^2 P_z^2) \\
& + \tilde{A}_{6i}^{(0)}(P_x^2 + P_y^2 + P_z^2)^3,
\end{aligned}
\tag{21}
$$

with parameter values in Table II. Figure 4 shows the temperature dependence of the polarization of PTO as obtained from $\tilde{F}_3$ and its comparison with second-principles data; the agreement is essentially perfect. The agreement remains perfect for model $\tilde{F}_4$.

By inspection of Table II, one can note that the best-performing models highlighted in this section share the majority of their couplings. This further supports the robustness of our approach and the physical meaningfulness of the interaction terms identified by our automatic ML procedure.

B. $F(\boldsymbol{P}, \boldsymbol{\eta}; \boldsymbol{\mathcal{E}}, \boldsymbol{\sigma}, T)$ models

We now consider models including strain, which we fit using the $\mathcal{D}$ training set described in Section III B. Figure 5 summarizes our results, i.e., the errors obtained from a direct minimization of E (a) and the validation error e (b). We focus on models containing between 11 and 17 parameters, which we find are reasonably accurate.

As in the case of the $\tilde{F}(\boldsymbol{P}; \boldsymbol{\mathcal{E}}, T)$ models, we find that the most accurate potentials (smallest E) are not the ones delivering most robust predictions (smallest e). As in the

previous section, we establish a threshold of $\mathsf{e} < 10^{-1}$ for the acceptable model accuracy, which corresponds to a maximum error of about 0.1 C m^{-2} for the predicted polarization and about 0.4% for the predicted strain. We find that the 14-parameter model labeled F_7 gives us an acceptable description of the system. We also see that, if we extend our analysis up to models with 17 parameters, we can keep improving the predictive error, models labeled F_8 and F_9 being two representative examples. Supplementary Figure 3 includes more details on how these models reproduce the TS data, and the mentioned models are fully specified in Table III.

Moving beyond 17 parameters involves consideration of a much larger number of models, and we did not pursue this systematically. Nevertheless, based on a partial exploration – by extending models with small E and low e errors –, we obtain evidence suggesting that the predictive error e is minimized for a model with 30 parameters.

If we inspect the electric and elastic contributions to E, it is apparent that the error is dominated by the elastic component (see Supplementary Note 1 and Supplementary Figure 4). In view of this, we experimented with reweighting the different contributions to E and e, but did not observe any significant change in the fitted models.

We also considered models with additional (higher order) strain, and found that our automatic procedure continues to select the same – simple and reasonably accurate – optimum potentials. Hence, we conclude that the way in which we combine the electric and elastic contributions to the error is sufficient to obtain reliable results.

If we turn to our optimum $F(\boldsymbol{P}, \boldsymbol{\eta}; \boldsymbol{\mathcal{E}}, \boldsymbol{\sigma}, T)$ models, we

TABLE III. Parameters of selected $F(\boldsymbol{P}, \boldsymbol{\eta}; \boldsymbol{\mathcal{E}}, \boldsymbol{\sigma}, T)$ models given in SI units.

	Parameter	Units	F_7	F_8	F_9
T-independent terms	$A_{2i}^{(0)}$	10^8 C^{-2} m^2 N	-3.81307	-3.17357	-3.11360
	$A_{4i}^{(0)}$	10^8 C^{-4} m^6 N	0.90945	0.56767	-1.62015
	$A_{22}^{(0)}$	10^8 C^{-4} m^6 N	-1.67506	-5.00439	-1.63859
	$A_{6i}^{(0)}$	10^8 C^{-6} m^{10} N	2.01344	2.58481	4.70951
	$A_{42}^{(0)}$	10^8 C^{-6} m^{10} N			-1.01874
	$A_{62}^{(0)}$	10^8 C^{-8} m^{14} N			-4.23945
	$B_{12}^{(0)}$	10^8 C^{-2} m^2 N	-69.23618	-99.33400	-70.24195
	$B_{14}^{(0)}$	10^8 C^{-4} m^6 N			-31.37833
	$B_{1',11}^{(0)}$	10^8 C^{-2} m^2 N	0.01283	0.01284	0.01283
	$C_1^{(0)}$	10^{11} m^{-2} N	-0.00068	0.00382	0.00293
	$C_2^{(0)}$	10^{11} m^{-2} N	0.81154	0.99169	1.04524
	$C_{11}^{(0)}$	10^{11} m^{-2} N	0.57923	0.61994	0.67598
	$C_{2'}^{(0)}$	10^{11} m^{-2} N	0.50354	0.50354	0.50354
T-depend. terms	$A_{2i}^{(1)}$	10^6 C^{-2} m^2 N K^{-1}	0.83591	0.74608	0.72419
	$A_{4i}^{(1)}$	10^6 C^{-4} m^6 N K^{-1}			0.38654
	$A_{22}^{(1)}$	10^6 C^{-4} m^6 N K^{-1}		0.75520	
	$A_{6i}^{(1)}$	10^6 C^{-6} m^{10} N K^{-1}			-0.14247
	$B_{12}^{(1)}$	10^6 C^{-2} m^2 N K^{-1}		3.86652	
	$C_1^{(1)}$	10^6 m^{-2} N K^{-1}	-2.50047	-3.68843	-3.78180

find that F_7 has the following form:

$$
\begin{aligned}
F_7 = {} & (A_{2i}^{(0)} + A_{2i}^{(1)}T)(P_x^2 + P_y^2 + P_z^2) \\
& + A_{4i}^{(0)}(P_x^2 + P_y^2 + P_z^2)^2 \\
& + A_{22}^{(0)}(P_x^2 P_y^2 + P_x^2 P_z^2 + P_y^2 P_z^2) \\
& + A_{6i}^{(0)}(P_x^2 + P_y^2 + P_z^2)^3 \\
& + B_{12}^{(0)}(\eta_{xx}P_x^2 + \eta_{yy}P_y^2 + \eta_{zz}P_z^2) \\
& + B_{1'11}^{(0)}(\eta_{yz}P_yP_z + \eta_{xz}P_zP_x + \eta_{xy}P_xP_y) \\
& + (C_1^{(0)} + C_1^{(1)}T)(\eta_{xx} + \eta_{yy} + \eta_{zz}) \\
& + C_2^{(0)}(\eta_{xx}^2 + \eta_{yy}^2 + \eta_{zz}^2) \\
& + C_{11}^{(0)}(\eta_{xx}\eta_{zz} + \eta_{yy}\eta_{xx} + \eta_{yy}\eta_{zz}) \\
& + C_{2'}^{(0)}(\eta_{yz}^2 + \eta_{xz}^2 + \eta_{xy}^2),
\end{aligned}
\tag{22}
$$

This model is equivalent to $\tilde{F}_3$ (Eq. (21)) in what regards the couplings involving the polarization alone, the temperature dependence being restricted to the quadratic parameter A_{2i}. Additionally, it contains the lowest-order elastic and polarization-strain couplings, resembling closely (and validating) the simple Landau-like potentials used in the literature.[27] It is also worth noting that this model includes, by construction, a term $C_1^{(1)}$ that accounts for a variation of the free energy that is linear on both strain and temperature. In essence, this term accounts for thermal expansion, which is of course present in our second-principles simulations. Interest-

ingly, this obviously important factor has never been considered explicitly, as far as we can tell, in phenomenological Landau-type treatments of ferroelectrics.

Figure 6 shows the temperature dependence of polarization and strain obtained by minimizing F_7, along with a comparison to the second-principles MC data. The agreement between the two datasets is essentially perfect, except for a noticeable deviation for the strain η_{zz} parallel to the polarization P_z. As for the further improved F_8 and F_9, as shown in Table III, they constitute an extension of F_7 and, most interestingly, they feature additional temperature-dependent parameters. In this case, as shown in Fig. 6, we obtain a perfect agreement between the TS and predicted data for the temperature-dependent order parameters at zero applied fields.

V. DISCUSSION

Having defined and applied our approach to compute optimal free energy potentials from thermodynamic data, now we discuss some additional aspects of our work and the opportunities it opens.

A. Non-trivial physical insights and predictions

In the burgeoning field of MLIPs, some groups are currently focusing on developing approaches that yield "interpretable" potentials.[6,8] Such efforts typically start by
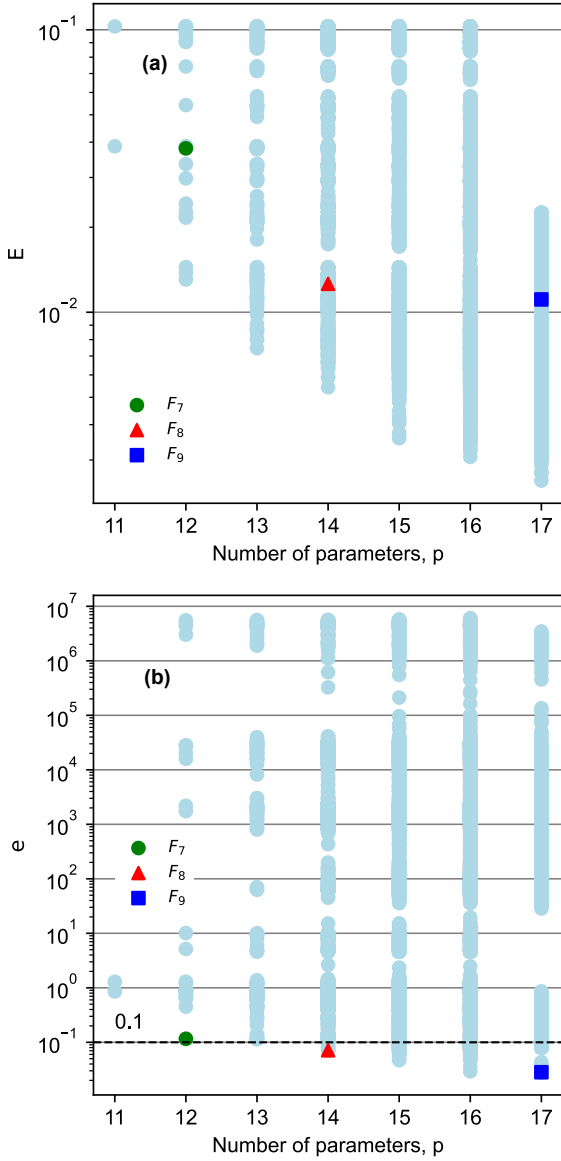
FIG. 5. (a) Error function E as a function of the polynomial degree p. (b) Predictive error e as a function of p. The dashed line indicates the 0.1 [arb. unit.] threshold. Coloured symbols highlight the selected models (F_7, F_8, and F_9) as shown in the legend.
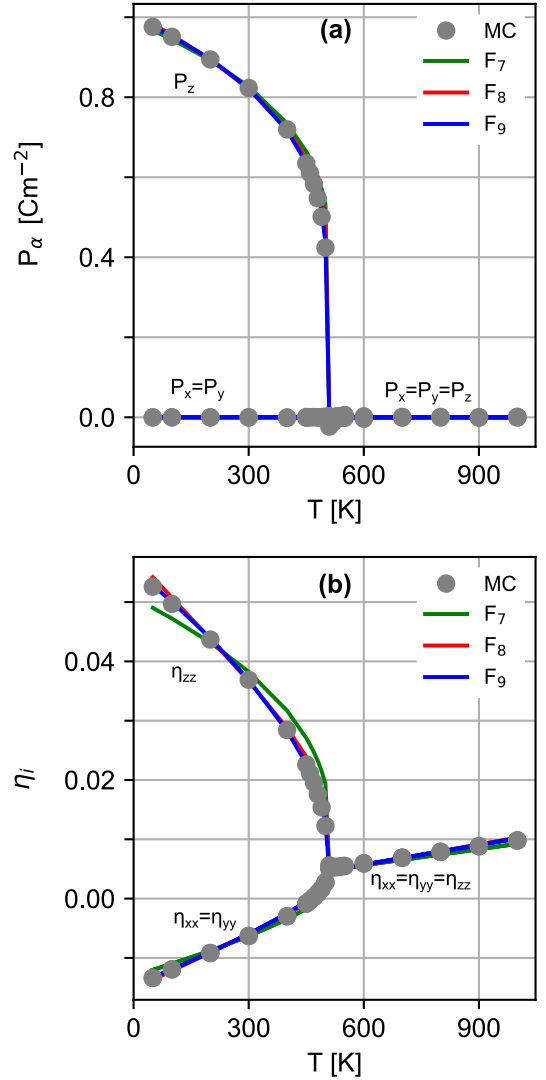

FIG. 6. Temperature dependence of polarization (a) and strain (b) components for the models indicated in the legend, which are compared against the second-principles Monte Carlo results in our TS (grey circles). Note that the polarization and temperature are given in SI units.

introducing a specific form of the potential – whose accuracy can be systematically improved, ideally – that is tailored to characterize the dominant interatomic interactions in terms of a relatively small number of parameters. Usually, such approaches take advantage of decades of work on effective models and force fields, and somehow constitute a culmination of those, powered by modern ML tools. We tend to include in this category diverse approaches ranging from those based on kernel[3] and many-body potentials[6] to the so-called "second-principles"[24,28] and "effective Hamiltonian"[35,36] methods based on a polynomial expansion of the energy around a reference structure. Beyond their physical

transparency (as compared to a generic neural network at least), such approaches enable a flexible compromise between the accuracy and the computational cost of the simulations. Further, we would argue that, the resulting models being comparatively simple, they can be expected to yield valuable predictions beyond the TS used to fit them. We have evidence of this from more than a decade of second-principles work on ferroelectric oxides,[28–31] and we are observing a similar pattern in ongoing projects where we use minimalist kernel-based MLIPs to investigate such structurally complex compounds.[37]

Our approach to compute free energy potentials is physics based and yields overly simple optimal models. Thus, the question naturally emerges: should we expect these models to predict non-trivial physical effects that

are not present in the TS data? To explore this matter, we recall the non-trivial behavior of PTO in what concerns the role of strain, as briefly summarized in Section III A. Let us consider such subtle couplings and check whether they are captured by our models. For the sake of concreteness, let us focus on the $\tilde{F}_4$ and F_7 potentials introduced above.

It has been long known from DFT simulations[27,28] that, if we constrain PTO to have the lattice vectors of the extrapolated cubic reference structure (which amounts to choosing $\boldsymbol{\eta} = \mathbf{0}$ in our description), this material displays a rhombohedral ground state with $P_x = P_y = P_z \neq 0$, rather than the usual tetragonal phase. Interestingly, PTO's tendency to display a tetragonal or rhombohedral state is governed by coupling terms like $\tilde{A}_{22}$ or A_{22}, which quantify, to the lowest order, the anisotropy of the energy landscape as a function of the polarization orientation. As can be seen from Table II, our $\tilde{F}_4$ model presents $\tilde{A}_{22} \approx 3 \times 10^8$ SI > 0, where the positive value of this parameter implies that a tetragonal state with $\boldsymbol{P} \parallel \langle 001 \rangle$ is favored over, e.g., rhombohedral variants with $\boldsymbol{P} \parallel \langle 111 \rangle$. By contrast, for F_7, Table III shows that the corresponding parameter is $A_{22} \approx -2 \times 10^8$ SI < 0; hence, according to this model, the occurrence of the polarization by itself – in the absence of strain – would yield a rhombohedral ground state for PTO. Indeed, in the case of F_7, we need to allow for polarization and strain to occur simultaneously in order to recover the well-known tetragonal ground state, as indeed shown in Fig. 6. We thus find that our free energy models capture the subtle polarization-strain couplings that determine the symmetry of the ferroelectric phase of PTO.[27,28] (See Ref. 27 for a deeper discussion on how the strain renormalizes the polarization energy landscape.)

Further, it is widely accepted that in ferroelectric perovskites like $PbTiO_3$ or $BaTiO_3$ the first-order character of the transition relies on the strain-polarization couplings.[35,38] It is also well-known that in simple Landau models – as those obtained from our optimization procedure – the character of the transition, continuous or discontinuous, depends on the sign of the $\tilde{A}_{4i}$ parameter, the transition being discontinuous when $\tilde{A}_{4i} < 0$.[13,21] Thus, it is no surprise to find, in Table II, that we obtain $\tilde{A}_{4i} \approx -0.6 \times 10^8$ SI < 0 for model $\tilde{F}_4$. As for model F_7, Table II shows that we obtain $A_{4i} \approx 0.9 \times 10^8$ SI > 0, suggesting that PTO should display a continuous ferroelectric phase transition if the strain is kept null. Thus, our simple models capture the polarization-strain couplings that control the nature – continuous vs. discontinuous – of PTO's ferroelectric phase transition.

Having established that our optimal models $\tilde{F}_4$ and F_7 capture well these expected behaviors at a qualitative level, one may wonder to what extent they are also quantitatively accurate. To test this, we perform second-principles Monte Carlo simulations of PTO under the $\boldsymbol{\eta} = \mathbf{0}$ elastic constraint. We obtain a phase transition at about 450 K, from cubic paraelectric to rhombohedral ferroelectric, marked by the spontaneous occurrence of a
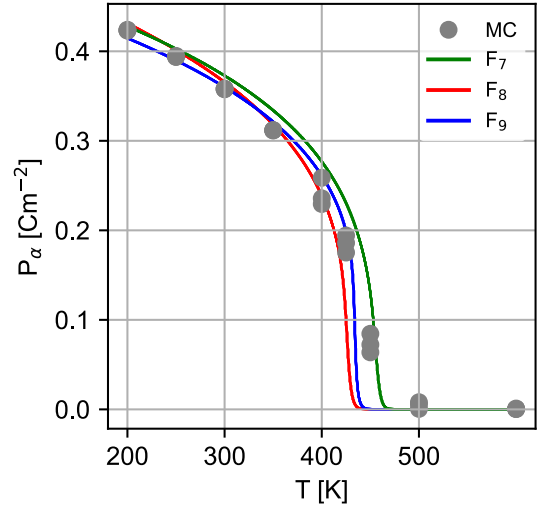

FIG. 7. Temperature dependence of the polarization components compared with the predictions of models F_7 (green), F_8 (red), and F_9 (blue) under the elastic condition $\boldsymbol{\eta} = \mathbf{0}$. Black markers represent second-principle data. Note that the polarization and temperature are given in SI units.

polarization along a $\langle 111 \rangle$ pseudocubic direction. Additionally, we consider the F_7, F_8, and F_9 models for $\boldsymbol{\eta} = \mathbf{0}$, and compute the minimum of the free energy as a function of temperature. The results from these calculations, shown in Fig. 7, display a remarkable agreement with the second-principles data. For example, the F_7 model is able to reproduce the continuous character of the transformation, and it also yields a transition temperature around 450 K. Thus, we find that F_7 predicts the system's behavior for $\boldsymbol{\eta} = \mathbf{0}$ very well, even at a quantitative level.

We thus find that our optimal models, $\tilde{F}_4$ and F_7, capture all the main physical effects associated to the strain-polarization coupling in a qualitatively correct way that is also physically transparent. Further, the F_7 model gives a fair quantitative description of our simulated PTO under the $\boldsymbol{\eta} = \mathbf{0}$ elastic constraint. This is a remarkable result, because the TS used to fit this model does not contain any information of the behavior of PTO in states satisfying, not even approximately, the $\boldsymbol{\eta} = \mathbf{0}$ condition (we checked that the configurations in $\mathcal{D}$ present strains with a magnitude of at least 0.5 %). This agreement strongly supports the choice of polynomial Landau-like models to capture, within ML schemes, the free energy potential of materials displaying non-reconstructive (typically, soft-mode driven) phase transitions, of which PTO is a representative example. More generally, these findings underscore the utility of physics-informed ML approaches and the remarkable predictive power such models can exhibit.

B. Peculiarities of this ML approach

Typical MLIP model-construction schemes rely on training, validation, and test datasets. The training set is used to compute the model parameters; the validation set is used to refine the choice of the hyperparameters that define the model or the training conditions; finally, the test set is used to estimate the accuracy of the model's predictions. The three datasets contain information that is equivalent in a statistical sense, i.e., they are usually composed of structures chosen at random from a single batch of data. (A rule of thumb is to use at least 60 % of the data for training, at least 10 % for validation, and at least 10 % for testing.) The approach employed here differs from this general protocol, which warrants some comments.

The only relevant hyperparameters in our construction scheme are the cut-offs (i.e., the choice of highest-order terms considered) in the expansion of the free energy as a function of polarization and strain components. Because of the mathematical simplicity of Landau potentials, it is trivial to work with cut-offs high enough as to make the universe of possible models essentially complete.

For a given choice of cut-offs (as, e.g., corresponding to the couplings listed in Table I), we are left with the task of identifying the specific couplings that yield an optimum potential that is (1) as simple as possible, (2) as accurate as required, and (3) as reliable (predictive) as possible. This can be considered a second-level choice of hyperparameters. As explained above, we deal with this task automatically by monitoring the predictive error e (Eq. (19)) and, typically, selecting the simplest model that yields e below a certain threshold. This procedure thus constitutes a model validation, but with some key differences with respect to the usual approach. First, in our validation strategy, we do not employ a different dataset to evaluate the models by computing the (fitting) error E. (As mentioned above, we do not find this strategy effective.) Rather, we consider the whole TS employed to fit the model parameters, but use the information in a different way. Specifically, we take advantage of the fact that all the states in the TS are stable equilibrium points, which implies that our model should be able to predict them as local free energy minima for the corresponding conditions of temperature, electric field and stress, as sketched in Fig. 1. By defining the error function e, which quantifies the accuracy of such a prediction, we implement a very demanding and informative validation criterion.

The error e corresponding to the validated model measures the maximum deviation we can expect when we use it in applications. Because the implemented validation procedure quantifies the predictive power of the models in an efficient manner that replicates the way in which the potentials will be used (that is, to compute equilibrium states in different conditions), we take it as a measure of the quality of our best model. Thus, within our scheme, the testing step is a byproduct of the validation step.

Given the usefulness of the predictive error e, one could wonder about the possibility of fitting the model's parameters by a direct minimization of this function. While possible in principle, this strategy suffers from a major disadvantage, namely, that we do not have a mathematical expression for e as a function of the model's parameters, let alone a formula for its derivatives with respect to said parameters. Hence, finding the minimum of e constitutes a challenging and computationally intensive numerical problem, to be contrasted with the simplicity of minimizing E (which boils down to the simple matrix operations in Eq. (14)). Thus, minimizing E for fitting – thus enabling the exploration of thousands of candidate models –, along with using e for validation (and testing), emerges as the most effective strategy.

In sum, we take advantage of the peculiarities of our TS and chosen models to implement validation and test steps that outperform the application of generic ML practices to our case. We contend that these ideas, or variations thereof, may be valuable and merit consideration in other contexts.

C. Predictive "third-principles" simulations

The present work is part of a longer-term effort to develop methods for mesoscale and macroscopic simulations of ferroic materials undergoing non-reconstructive phase transitions, a large family that includes many all-important ferroelectric and ferroelastic compounds. Traditionally, such simulations have relied on empirical Landau (macroscopic) and Ginzburg-Landau (mesoscopic) models. The present work addresses the question of whether such schemes may serve us as a basis to build potentials that can be improved systematically, capable of accounting for large sets of data that can be obtained from more basic and predictive simulations (as done here), from experiment, or eventually by combining both. The successful application to PTO, a less than trivial compound, suggests that polynomial Landau-type potentials are indeed a valid choice.

The next step in this program would be the generalization of the Landau models to situations where the order parameters can present a spatial variation (i.e., non-zero gradients), a key development that would enable the study of multidomain states. Such Ginzburg-Landau models would be fitted to data from atomistic simulations that capture thermodynamic properties of multidomain configurations. The key step in the procedure is to implement a mapping between the atomic configurations in the dataset and the order-parameter fields in the Ginzburg-Landau potential. This problem has already been discussed in the literature and field models for very complex compounds (e.g., $PbZrO_3$) have been derived in the limit of 0 K.[19,20] While an application at finite temperatures involves some subtleties, the work plan is in principle clear. Additionally, it should be noted that for comparatively simple compounds – like $PbTiO_3$ or $BaTiO_3$ – it is

conceivable to estimate the parameters of the most relevant gradient terms from experimental information, e.g., concerning the width of domain walls.[15,16]

Having said this, we believe that the most important and least obvious step of this longer-term program pertains to the dynamical behavior of the order parameters, be they treated as macroscopic quantities or position-dependent fields. Indeed, the community has traditionally employed effective time-evolution equations based on Landau or Ginzburg-Landau potentials, of the form

$$\mu\ddot{Q} + \gamma\dot{Q} = -\frac{\partial F}{\partial Q} , \qquad (23)$$

where μ and γ are effective inertial and damping constants, respectively, and Q is a generic order parameter.[10] Usually, such an equation is considered in the overdamped limit and is just used as a numerical tool to find minima of F. In such a context, the particular choice of μ and γ is largely irrelevant, and authors assume $\mu = 0$ and $\gamma = 1$ in the vast majority of studies. However, the situation is quickly changing. Because of a growing interest in the response of complex electric and elastic textures to time dependent fields, including ultra-fast electric probes where the inertia of the polarization order parameter becomes relevant,[39,40] the question of how to compute realistic values for the effective dynamic constants is starting to receive attention. Indeed, schemes to derive such parameters from more fundamental (atomistic) simulations are beginning to appear,[41,42] and this problem will also be the focus of an upcoming article from our group. Let us stress that, as regards such effective dynamic constants, it may be possible to draw sensible values from experiment in some cases – e.g., dielectric and infrared spectroscopy may offer relevant information about the γ parameter for the polarization field.[40] However, whenever we deal with a structural order parameter that cannot be easily probed experimentally – e.g., the strain field, or the tilts of oxygen octahedra that control the structural behavior of most perovskite oxides[43] –, a theoretical approach to this problem becomes essential.

Thus, the present work is best understood as part of a larger effort to develop predictive simulation methods at mesoscopic and macroscopic scales. In earlier work, some of us introduced the term "second principles" to denote atomistic lattice-dynamical potentials formulated as polynomial expansions around physically relevant reference structures.[24,28,44] In the same spirit, we now propose the term "third principles" to describe the non-atomistic Landau and Ginzburg-Landau approaches discussed here. These third-principles methods also rely on a polynomial expansion around an appropriate reference state, which renders physically transparent and computationally light models. As shown in this work, such an approximation may be sufficiently accurate.

VI. SUMMARY AND CONCLUSIONS

In this work we introduce a scheme to build Landau-like free energy potentials suitable to describe non-reconstructive phase transitions, as those displayed by most ferroelectric and ferroelastic materials. The method is general and can be applied to any such compound – from classic perovskite oxides like $PbTiO_3$, $BaTiO_3$ or $BiFeO_3$, to novel van der Waals ferroelectrics like hexagonal-BN[45] and many chalcogenides[46] – as long as one is able to generate relevant thermodynamic data (e.g., polarizations and strains as a function of temperature and applied fields) from a more fundamental – atomistic – theory. Further, the present approach is also suitable for use with experimental data.

This method complements statistical simulations based on machine-learned interatomic potentials, and it can be used – in an essentially routine manner – to derive Landau models from those. Our approach is useful to shed light on the behavior of complex materials, by deriving physically transparent Landau potentials that describe their phase transitions in terms of a few relevant couplings. Further, it enables a first necessary step towards predictive dynamical simulations, at the mesoscopic or macroscopic scales, based on Landau or Ginzburg-Landau models. Indeed, this work is part of a longer-term effort to develop what we call predictive "third-principles" methods.

We have demonstrated our approach with an application to ferroelectric perovskite $PbTiO_3$. By introducing an original model-validation step, which tests the predictive power of the potentials and yields a relevant numerical estimate of their accuracy, our machine-learning scheme makes it possible to automatically identify models that strike an optimum balance between accuracy, predictive power, and simplicity. We have shown that the identified optimal Landau potentials capture all the physical effects described in the training set (i.e., the non-reconstructive and weakly discontinuous structural transition of $PbTiO_3$; the system's response to applied electric fields and stresses) in a quantitative correct manner, while offering direct insights into the underlying physical couplings. Remarkably, our models also capture subtle physical phenomena – concerning the non-trivial coupling between electric polarization and elastic strains in $PbTiO_3$ – in a way that is qualitatively and quantitatively correct, while remaining physically transparent. Indeed, we show that the good performance of our optimum models extends to effects (e.g., the behavior of $PbTiO_3$ under peculiar elastic boundary conditions) that are not present in the training set used to fit them. In our view, this can be partly attributed to their overly simple and physically motivated form, and we contend it is probably an example of the predictive power of a broader class of physics-informed machine-learned potentials.

---

[1] Albert P. Bartók and Gábor Csányi, "Gaussian approximation potentials: A brief tutorial introduction," International Journal of Quantum Chemistry **115**, 1051–1057 (2015).

[2] Han Wang, Linfeng Zhang, Jiequn Han, and Weinan E, "DeePMD-kit: A deep learning package for many-body potential energy representation and molecular dynamics," Computer Physics Communications **228**, 178–184 (2018).

[3] Ryosuke Jinnouchi, Ferenc Karsai, and Georg Kresse, "On-the-fly machine learning force field generation: Application to melting points," Phys. Rev. B **100**, 014105 (2019).

[4] Zheyong Fan, Zezhu Zeng, Cunzhi Zhang, Yanzhou Wang, Keke Song, Haikuan Dong, Yue Chen, and Tapio Ala-Nissila, "Neuroevolution machine learning potentials: Combining high accuracy and low cost in atomistic simulations and application to heat transport," Physical Review B **104**, 104309 (2021).

[5] Albert Musaelian, Simon Batzner, Anders Johansson, Lixin Sun, Cameron J. Owen, Mordechai Kornbluth, and Boris Kozinsky, "Learning local equivariant representations for large-scale atomistic dynamics," Nature Communications **14**, 579 (2023).

[6] Stephen R. Xie, Matthias Rupp, and Richard G. Hennig, "Ultra-fast interpretable machine-learning potentials," npj Computational Materials **9**, 162 (2023).

[7] Ilyes Batatia, Philipp Benner, Yuan Chiang, Alin M. Elena, Dávid P. Kovács, Janosh Riebesell, Xavier R. Advincula, Mark Asta, Matthew Avaylon, William J. Baldwin, Fabian Berger, Noam Bernstein, Arghya Bhowmik, Samuel M. Blau, Vlad Cărare, James P. Darby, Sandip De, Flaviano Della Pia, Volker L. Deringer, Rokas Elijošius, Zakariya El-Machachi, Fabio Falcioni, Edvin Fako, Andrea C. Ferrari, Annalena Genreith-Schriever, Janine George, Rhys E. A. Goodall, Clare P. Grey, Petr Grigorev, Shuang Han, Will Handley, Hendrik H. Heenen, Kersti Hermansson, Christian Holm, Jad Jaafar, Stephan Hofmann, Konstantin S. Jakob, Hyunwook Jung, Venkat Kapil, Aaron D. Kaplan, Nima Karimitari, James R. Kermode, Namu Kroupa, Jolla Kullgren, Matthew C. Kuner, Domantas Kuryla, Guoda Liepuoniute, Johannes T. Margraf, Ioan-Bogdan Magdău, Angelos Michaelides, J. Harry Moore, Aakash A. Naik, Samuel P. Niblett, Sam Walton Norwood, Niamh O'Neill, Christoph Ortner, Kristin A. Persson, Karsten Reuter, Andrew S. Rosen, Lars L. Schaaf, Christoph Schran, Benjamin X. Shi, Eric Sivonxay, Tamás K. Stenczel, Viktor Svahn, Christopher Sutton, Thomas D. Swinburne, Jules Tilly, Cas van der Oord, Eszter Varga-Umbrich, Tejs Vegge, Martin Vondrák, Yangshuai Wang, William C. Witt, Fabian Zills, and Gábor Csányi, "A foundation model for atomistic materials chemistry," arXiv.2401.00096 (2024), 10.48550/arXiv.2401.00096.

[8] Ryan Jacobs, Dane Morgan, Siamak Attarian, Jun Meng, Chen Shen, Zhenghao Wu, Clare Yijia Xie, Julia H. Yang, Nongnuch Artrith, Ben Blaiszik, Gerbrand Ceder, Kamal Choudhary, Gabor Csanyi, Ekin Dogus Cubuk, Bowen Deng, Ralf Drautz, Xiang Fu, Jonathan Godwin, Vasant Honavar, Olexandr Isayev, Anders Johansson, Boris Kozinsky, Stefano Martiniani, Shyue Ping Ong, Igor Poltavsky, KJ Schmidt, So Takamoto, Aidan P. Thompson, Julia Westermayr, and Brandon M. Wood, "A practical guide to machine learning interatomic potentials – Status and future," Current Opinion in Solid State and Materials Science **35**, 101214 (2025).

[9] Hong-Liang Hu and Long-Qing Chen, "Three-dimensional computer simulation of ferroelectric domain formation," Journal of the American Ceramic Society **81**, 492–500 (1998).

[10] Long-Qing Chen, "Phase-field method of phase transitions/domain structures in ferroelectric thin films: A review," Journal of the American Ceramic Society **91**, 1835–1844 (2008).

[11] Pierre Toledano and Jean-Claude Toledano, *Landau theory of phase transitions* (World Scientific Publishing Company, 1987).

[12] Premi Chandra and Peter B. Littlewood, "A landau primer for ferroelectrics," in *Physics of Ferroelectrics: A Modern Perspective* (Springer Berlin Heidelberg, Berlin, Heidelberg, 2007) pp. 69–116.

[13] A.F. Devonshire, "Theory of ferroelectrics," Advances in Physics **3**, 85–130 (1954).

[14] M. J. Haun, E. Furman, S. J. Jang, H. A. McKinstry, and L. E. Cross, "Thermodynamic theory of $PbTiO_3$," Journal of Applied Physics **62**, 3331–3338 (1987).

[15] A. Tagantsev, L. E. Cross, and J. Fousek, *Domains in Ferroic Crystals and Thin Films* (Springer, 2010).

[16] Dennis Meier, Jan Seidel, Marty Gregg, and Ramamoorthy Ramesh, *Domain Walls: From Fundamental Properties to Nanotechnology Concepts* (Oxford University Press, 2020).

[17] Jorge Íñiguez, S. Ivantchev, J. M. Perez-Mato, and Alberto García, "Devonshire-landau free energy of batio$_3$ from first principles," Phys. Rev. B **63**, 144103 (2001).

[18] Anil Kumar and Umesh V. Waghmare, "First-principles free energies and ginzburg-landau theory of domains and ferroelectric phase transitions in $BaTiO_3$," Phys. Rev. B **82**, 054117 (2010).

[19] Andrea Schiaffino and Massimiliano Stengel, "Macroscopic polarization from antiferrodistortive cycloids in ferroelastic $SrTiO_3$," Phys. Rev. Lett. **119**, 137601 (2017).

[20] Konstantin Shapovalov and Massimiliano Stengel, "Tilt-driven antiferroelectricity in $PbZrO_3$," Physical Review Materials **7**, L071401 (2023).

[21] L. D. Landau and E. M. Lifshitz, *Statistical Physics, Part 1*, 3rd ed., Course of Theoretical Physics, Vol. 5 (Pergamon Press, Oxford, 1980).

[22] Darrell G. Schlom, Long-Qing Chen, Chang-Beom Eom, Karin M Rabe, Stephen K Streiffer, and Jean-Marc Triscone, "Strain tuning of ferroelectric thin films," Annual Review of Materials Research **37**, 589 (2007).

[23] William H. Press, Saul A. Teukolsky, William T. Vetterling, and Brian P. Flannery, *Numerical Recipes 3rd Edition: The Art of Scientific Computing*, 3rd ed. (Cambridge University Press, 2007).

[24] Carlos Escorihuela-Sayalero, Jacek C. Wojdeł, and Jorge

Íñiguez, "Efficient systematic scheme to construct second-principles lattice dynamical models," Phys. Rev. B **95**, 094115 (2017).

[25] Trevor Hastie, Robert Tibshirani, and Jerome Friedman, *The Elements of Statistical Learning: Data Mining, Inference, and Prediction*, 2nd ed. (Springer, 2009).

[26] Karin M. Rabe, Charles H. Ahn, and Jean-Marc Triscone, eds., *Physics of Ferroelectrics: A Modern Perspective* (Springer Berlin Heidelberg, Berlin, Heidelberg, 2007).

[27] R. D. King-Smith and David Vanderbilt, "First-principles investigation of ferroelectricity in perovskite compounds," Physical Review B **49**, 5828 (1994).

[28] Jacek C Wojdeł, Patrick Hermet, Mathias P Ljungberg, Philippe Ghosez, and Jorge Íñiguez, "First-principles model potentials for lattice-dynamical studies: general methodology and example of application to ferroic perovskite oxides," Journal of Physics: Condensed Matter **25**, 305401 (2013).

[29] Jacek C Wojdeł and Jorge Íñiguez, "Ferroelectric transitions at ferroelectric domain walls found from first principles," Physical Review Letters **112**, 247603 (2014).

[30] Pavlo Zubko, Jacek C Wojdeł, Marios Hadjimichael, Stéphanie Fernandez-Pena, Anaïs Sené, Igor Luk'yanchuk, Jean-Marc Triscone, and Jorge Íñiguez, "Negative capacitance in multidomain ferroelectric superlattices," Nature **534**, 524–528 (2016).

[31] M. A. Pereira Gonçalves, Carlos Escorihuela-Sayalero, Pablo Garca-Fernández, Javier Junquera, and Jorge Íñiguez, "Theoretical guidelines to create and tune electric skyrmion bubbles," Science Advances **5**, eaau7023 (2019).

[32] S. Das, Y. L. Tang, Z. Hong, M.A.P. Gonçalves, M.R. McCarter, C. Klewe, K.X. Nguyen, F. Gómez-Ortiz, P. Shafer, E. Arenholz, V.A. Stoica, S.-L. Hsu, B. Wang, C. Ophus, J.F. Liu, C.T. Nelson, S. Saremi, B. Prasad, A.B. Mei, D.G. Schlom, J. Íñiguez, P. García-Fernández, D.A. Muller, L.Q. Chen, J. Junquera, Martin L.W., and R. Ramesh, "Observation of room-temperature polar skyrmions," Nature **568**, 368–372 (2019).

[33] M. Graf and J. Íñiguez, "A unified perturbative approach to electrocaloric effects," Communications Materials **2**, 60 (2021).

[34] Jacek C Wojdeł and Jorge Íñiguez, "Testing simple predictors for the temperature of a structural phase transition," Physical Review B **90**, 014105 (2014).

[35] W. Zhong, David Vanderbilt, and K. M. Rabe, "First-principles theory of ferroelectric phase transitions for perovskites: The case of BaTiO$_3$," Physical Review B **52**, 6301 (1995).

[36] Xingyue Ma, Hongying Chen, Ri He, Zhanbo Yu, Sergei Prokhorenko, Zheng Wen, Zhicheng Zhong, Jorge Íñiguez-González, L. Bellaiche, Di Wu, and Yurong Yang, "Active learning of effective Hamiltonian for super-large-scale atomic structures," npj Computational Materials **11**, 70 (2025).

[37] Iñigo Robredo, Binayak Mukherjee, Hugo Aramberri, and Jorge Íñiguez-González, "Minimalist machine-learned interatomic potentials can predict complex structural behaviors ac¡curately," In preparation (2025).

[38] U. V. Waghmare and K. M. Rabe, "Ab initio statistical mechanics of the ferroelectric phase transition in PbTiO$_3$," Physical Review B **55**, 6161 (1997).

[39] Tiannan Yang, Bo Wang, Jia-Mian Hu, and Long-Qing Chen, "Domain dynamics under ultrafast electric-field pulses," Phys. Rev. Lett. **124**, 107601 (2020).

[40] Taorui Chen, Bo Wang, Yujie Zhu, Shihao Zhuang, Long-Qing Chen, and Jia-Mian Hu, "Analytical model and dynamical phase-field simulation of terahertz transmission across ferroelectrics," Phys. Rev. B **109**, 094305 (2024).

[41] Jianyi Liu, Haohua Wen, Weijin Chen, and Yue Zheng, "Atomistic studies of temporal characteristics of polarization relaxation in ferroelectrics," Physical Review B **103**, 014308 (2021).

[42] Haohua Wen, Jianyi Liu, Jinhong Li, Bowen Li, Weijin Chen, and Yue Zheng, "A review of progress in theoretical modeling of polarization dynamics in ferroelectric materials," Journal of Physics: Condensed Matter **37**, 173003 (2025).

[43] Peng Chen, Mathieu N. Grisolia, Hong Jian Zhao, Otto E. González-Vázquez, L. Bellaiche, Manuel Bibes, Bang-Gui Liu, and Jorge Íñiguez, "Energetics of oxygen-octahedra rotations in perovskite oxides from first principles," Physical Review B **97**, 024113 (2018).

[44] Pablo García-Fernández, Jacek C Wojdeł, Jorge Íñiguez, and Javier Junquera, "Second-principles method for materials simulations including electron and lattice degrees of freedom," Physical Review B **93**, 195137 (2016).

[45] Menghao Wu and Ju Li, "Sliding ferroelectricity in 2D van der Waals materials: Related physics and future opportunities," Proceedings of the National Academy of Sciences **118**, e2115703118 (2021).

[46] Alexey Lipatov, Pradeep Chaudhary, Zhao Guan, Haidong Lu, Gang Li, Olivier Crégut, Kokou Dodzi Dorkenoo, Roger Proksch, Salia Cherifi-Hertel, Ding-Fu Shao, Evgeny Y. Tsymbal, Jorge Íñiguez, Alexander Sinitskii, and Alexei Gruverman, "Direct observation of ferroelectricity in two-dimensional MoS$_2$," npj 2D Materials and Applications **6**, 18 (2022).